SURFACE ROUGHNESS AND SIZE MEASUREMENTS OF MICROSCOPIC PARTICLES BY REFLECTION INTERFERENCE CONTRAST MICROSCOPY

An Undergraduate Research Scholars Thesis

by

JAMISON CHANG

Submitted to Honors and Undergraduate Research
Texas A&M University
in partial fulfillment of the requirements for the designation as

UNDERGRADUATE RESEARCH SCHOLAR

Approved by
Research Advisor: Dr. Victor Ugaz

May 2013

Major: Chemical Engineering

TABLE OF CONTENTS

Page

TABLE OF CONTENTS..1

ABSTRACT..2

ACKNOWLEDGEMENTS..3

CHAPTER

I INTRODUCTION………………………………………………………………......4

II METHODS…………………………………………………………………….. 8

Image acquisition and computations……………………………………………...8
Sample selection and preparation……………………........………..……...…. 8
Methodology………………………………………………………………...... 10
Image processing……………………………………………………….........11
Surface roughness modeling………………………………………………...... 12
Roughness effects on intensity computations…………………………………… 13
Simulated intensity vs. height curve………………………………………….…..... 14
Statistical methods………………………………………………………………. 17

III RESULTS..……………………………………………………………………18

Image processing improvements……………………………………………....18
Characterization of surface roughness simulations…………………………..…..24
Simulated intensity vs. height curve…………………………………………….. 28
Particle size and minimum separation distance measurements…………………. 34

IV CONCLUSION…………………………………………………………………. 36

REFERENCES.. 38

ABSTRACT

Surface Roughness and Size Measurements of Microscopic Particles by Reflection Interference Contrast Microscopy. (May 2013)

Jamison Chang
Department of Chemical Engineering
Texas A&M University

Research Advisor: Dr.Victor Ugaz
Department of Chemical Engineering

Accurate information about particle roughness and the deformation that occurs when a particle is in contact with a surface is needed to provide improved models of particle resuspension and adhesion. The capabilities of reflection interference contrast microscopy (RICM) in particle roughness measurements are explored in this study, by measuring the minimum separation distance between the particle and a flat substrate and possible roughness effects on the visibility of interference fringes. Monodisperse samples of polystyrene latex and glass beads were studied in order to compare surface roughness of different types of particles of similar size. Polydisperse samples of glass beads were also analyzed to compare particle size and surface roughness. Particle size and minimum separation distance values were measured with RICM taking into account surface roughness effects. It was shown that particle size data can be accurately obtained by RICM analysis, and the minimum separation distance that is measured by RICM can be used to show differences in surface roughness between different types of particles.

ACKNOWLEDGMENTS

I would like to acknowledge Dr. Ugaz for agreeing to advise me on this project, for his encouragement, and for his recommendations. I would also like to thank Jose C. Contreras-Naranjo for his guidance and instruction during the course of this project.

CHAPTER I

INTRODUCTION

Several factors play a significant role in particle adhesion and resuspension phenomena and improved models are important in many areas, including dispersion of contaminants, which affects air quality, semiconductors, and drug delivery (1). For instance, it is known that different deposition mediums produce varying effects on the adhesion and resuspension of particles from a flat substrate (1), which can possibly be explained following a detailed microscopic description of the phenomenon, as follows. When particles are deposited using a liquid medium, a liquid meniscus can form between the particles and the substrate during the drying process. Depending on the conditions of the drying, the meniscus will dry out totally or partially and the particles can undergo deformation due to capillary forces and van der Waals forces, creating different deposition scenarios with varying adhesion forces and, consequently, affecting particle resuspension. The van der Waals force occurs between the substrate and the particle once the particle is close enough to the surface and the capillary force is caused by the liquid meniscus; these forces can be modeled in the cases of deformed or undeformed spheres, including parameters such as particle size, contact area, separation distance between the particle and the surface, the surface tension of the liquid, and the liquid-sphere and liquid-glass contact angles (1). Therefore, a detailed microscopic description of deposition scenarios along with a nonoscopic characterization of the particles involved can provide a more appropriate input to existing adhesion and resuspension models or lead to new and more accurate formulations of the problem.

Reflection interference contrast microscopy (RICM) (2) offers a unique and convenient view of the deposition phenomenon previously described, given that critical parameters such as the minimum separation distance between particle and substrate, contact area, particle contour next to the contact area (3), and the presence of a liquid phase underneath the particles can be accurately quantified when looking at the sample from below (see Figure 1). The ability of RICM to measure the distance between surfaces with "nanometric precision" with a resolution of up to 1 nm (2) is very important in this context. Many mathematical models for adhesion and resuspension are limited to smooth surfaces, where the expected separation distance is zero, and models for microparticles have significant differences when compared with experimental data. Previous work has been done to account for the effects of surface roughness for these models, and the agreement between the models and experimental data improves greatly (4). As illustrated in Figure 1, the minimum separation distance (MSD) between the particle and a flat substrate can potentially be used to estimate particle roughness. Therefore, the main goal of the present research is to perform accurate separation distance measurements between particles and a flat substrate using RICM and determine possible correlations of these measurements with particle roughness. The results obtained will provide key information in terms of particle characterization and parameters required for adhesion and resuspension models.

The effect of MSD on the RICM images and the intensity profiles is depicted in Figure 1b-d. Previous work with RICM has shown that particle size and MSD can be quantified (5). However, data previously obtained can be more accurately analyzed with improved methods so that better measurements of particle size and precise models of particle roughness can be formulated. Areas of focus are to improve the image analysis by locating the center of the particle more accurately,

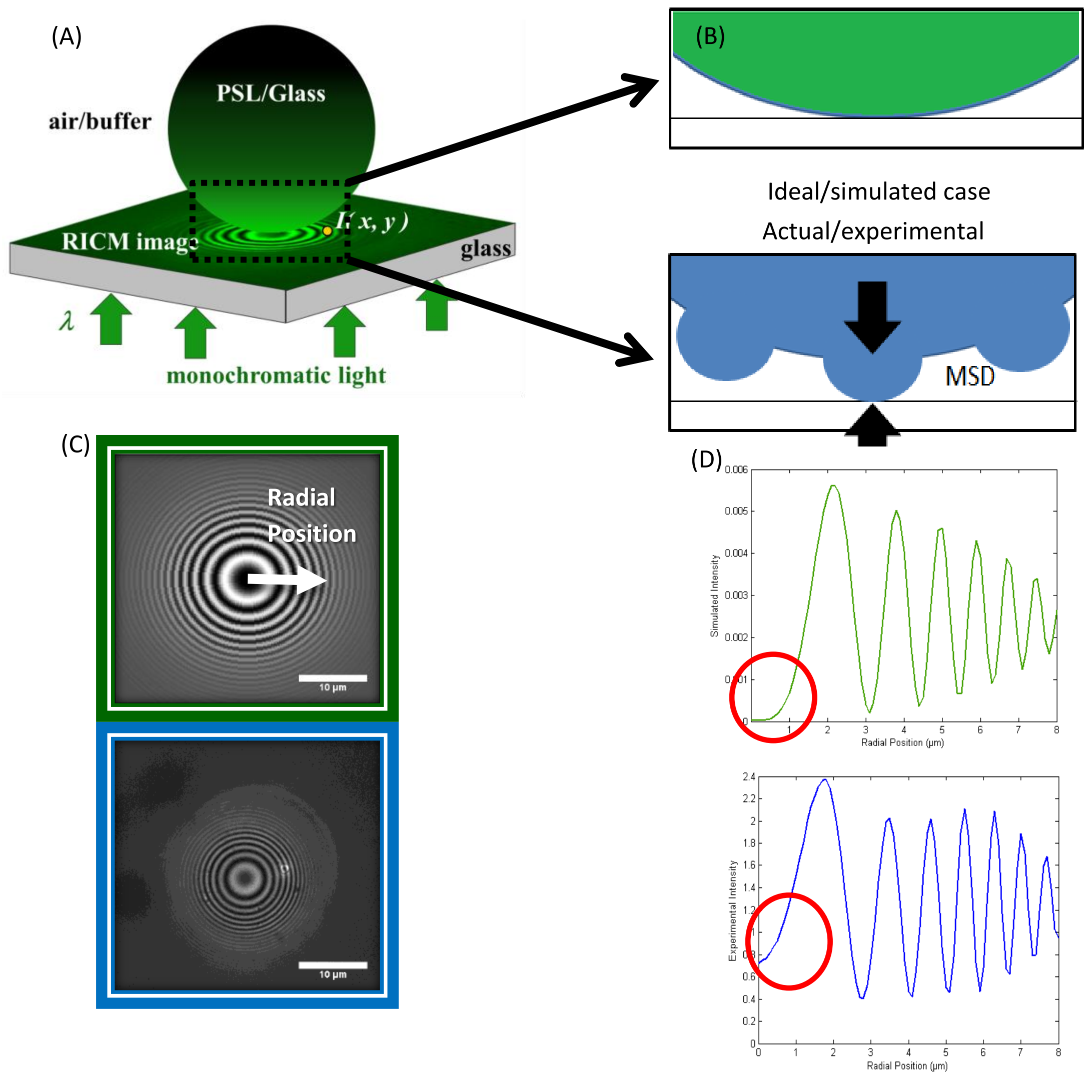

Figure 1. (A) Visual representation of RICM setup. (B) Comparison of an ideal/simulated (top) particle with an actual/experimental particle (bottom), as well as a depiction of MSD. (C) Comparison of RICM images from ideal (green) and experimental cases (blue) and radial position is illustrated in red. (D) Comparison of simulated intensity and experimental intensity profiles. The area of the intensity profile that shows the difference in MSD is circled in red.

given that MSD values are measured at the center of the interferograms; to accurately account for the asperity size and surface coverage effects on the RICM intensities; and to determine potential correlations between surface roughness and visibility of the RICM interference fringes. Also, once RICM is set up, the technique is easily implemented and large samples of data can be collected cheaply and quickly compared to other techniques such as scanning electron

microscopy (SEM). One criterion for comparing RICM to other surface roughness measurement techniques is to compare the vertical and horizontal resolution and size range limitations (Table 1).

Table 1. Comparison of techniques for measuring particle size and surface roughness of spheres.

Particle Size		
Method	Size Range	Description/Comment
Reflection Interference Contrast Microscopy[2]	1-1000 μm	provides unique view from bottom of particle, able to measure large polydisperse sample sizes quickly
Dynamic Light Scattering[6]	0.005–1 μm	measurement time: 1 min; no calibration needed; small amounts of noise cause large errors; small particles only; samples-suspensions and emulsions
TEM[7]	Nanometers	able to measure <10 nm particle size; higher magnification limits sample size; bias or errors up to 30%-50% of particle size
Electrical Sensing Zone[6]	0.5–1,000 μm	measurement time: 1-5 min; large particle counts; limitations: samples need to be suspended in conductive liquid
Optical Microscope[8]	0.5 to 40 μm	uncertainty: 0.056 μm per sphere; limited to monodisperse
Laser diffraction[6]	0.1-3000 μm	measurement time: < 30 sec; limited by range of particle concentrations required; no calibration

Surface Roughness of Sphere			
Method	Horizontal Resolution (nm)	Vertical Resolution (nm)	Limitations
Reflection Interference Contrast Microscopy[2]	~200	1	poorly reflecting surfaces
Scanning Tunneling Microscopy[9,12]	0.2	0.02	requires a conducting surface, small scanning area
Scanning Electron Microscope[9,12]	5	10-50	expensive, vacuum, small scanning area
Optical Interference[10]	500-1000	0.1-1	poorly reflecting surfaces
Atomic Force Microscope[11,12]	0.2-1	0.02	small scanning area

CHAPTER II

METHODS

Image acquisition and computations

The RICM microscope setup employed consisted of a Zeiss Axiovert 200 M inverted microscope with a 103 W HBO mercury vapor lamp and a Zeiss AxioCam mRm camera. A Zeiss Antiflex EC Plan-Neofluar 63x/1.25 Oil Ph3 objective was used with a 5 nm bandpass filer to obtain monochromatic green light of 546.1 nm. SEM images were taken by Dr. Yordanos Bisrat at the Materials Characterization Facility at Texas A&M University using an ultra-high resolution field emission scanning electron microscope (FE-SEM), the JEOL JSM-7500F. Computer code was provided by Jose C. Contreras-Naranjo in the Ugaz Research Group and computations were implemented in ImageJ (developed by the National Institutes of Health), using ordinary laptops, and MATLAB (developed by Mathworks), using up to eight processors in the Computer Cluster at the Chemical Engineering Department at Texas A&M University.

Sample selection and preparation

The monodisperse polystyrene latex particles that were used in the experiments were 15 µm in diameter with a refractive index of 1.59 and were manufactured by Thermo Scientific (PSL 15). The monodisperse glass beads that were used in the experiments were 15 µm in diameter and were provided by the Aerosol Technology Lab at Texas A&M University (Glass 15). The polydisperse glass beads 10-30 µm (Glass 10-30) and 30-50 µm (Glass 30-50) were both manufactured by Polysciences, made of soda lime glass, and both had a refractive index of 1.51. These particles are selected for observation because they offer features of different sizes at the

nanoscale, as evident from SEM images of PSL 15, Glass 10-30, and Glass 30-50 shown in Figure 2; these features are expected to induce a finite separation distance between the particles and a flat substrate.

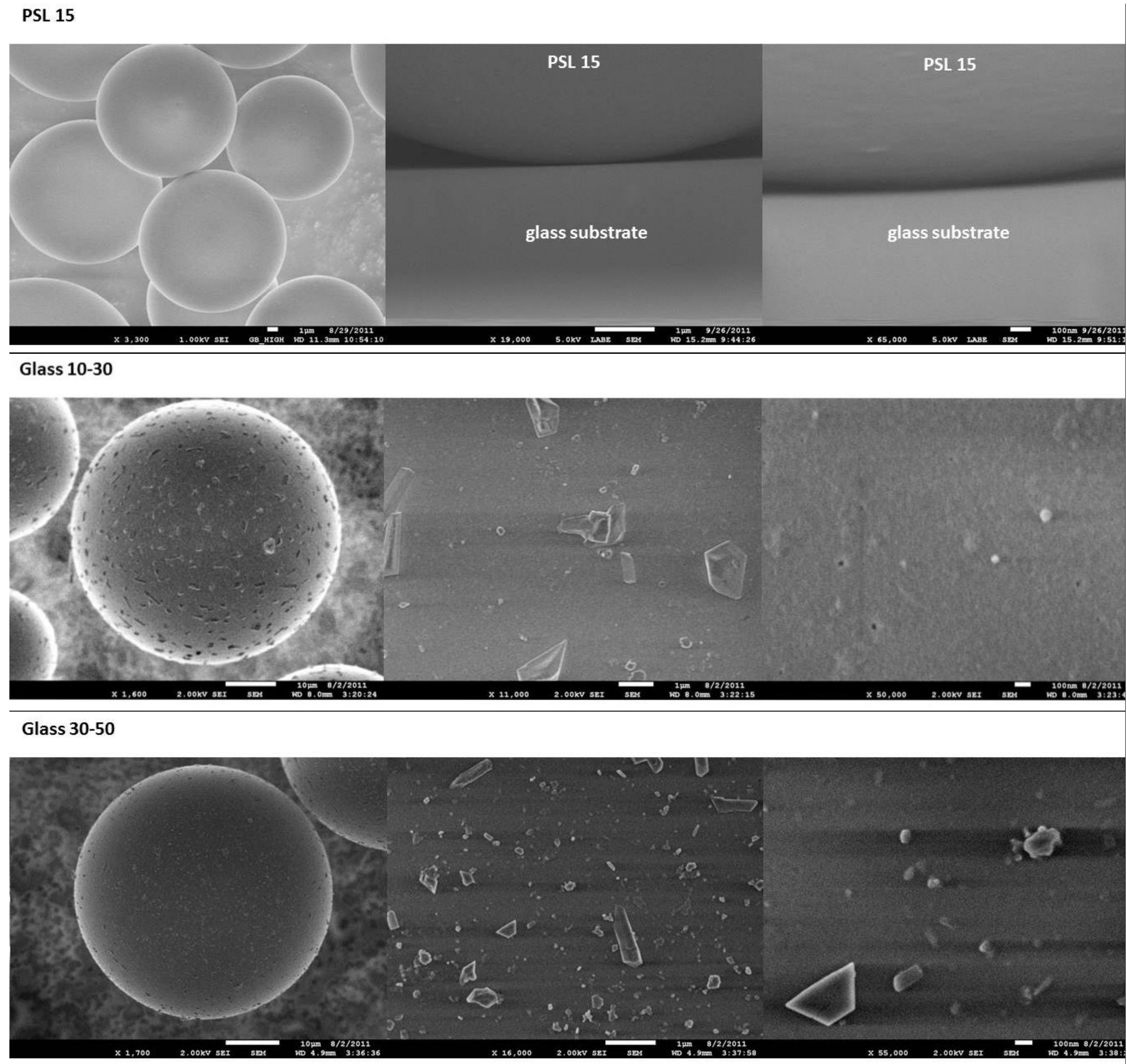

Figure 2. Scanning Electron Microscope images of Polystyrene Latex (15 µm diameter) and Glass beads (10-30 µm diameter and 30-50 µm diameter polydisperse) sample. Images were taken by Dr. Yordanos Bisrat at the Materials Characterization Facility at Texas A&M University.

Particles were placed on top of an optical borosilicate cover glass (0.16 to 0.19 mm thickness) in a medium of 0.1 M NaCl solution. Sodium chloride was added in order to allow the particle to come into contact with the cover glass, so the particle does not fluctuate. Prior to taking any RICM data, the lamp is allowed to warm up for one hour, in order to ensure that the intensity from the light source is consistent throughout the experiment. Several images of a cover glass exposed to air and without particles are taken for background subtraction. Then, the particle is observed using the RICM technique (making sure only a few particles appear in the field of view simultaneously) and an interferogram like the one shown in Figure 1c is obtained.

Methodology

Figure 3 provides an overview of the methodology followed and illustrates how the current work relates to previous measurements. In previous experiments (5), RICM images of particles were taken and processed using ImageJ; then, particle size was measured using surface profile reconstruction methods that were in the development stage and now perform with significantly improved nanometric accuracy, and surface roughness was estimated from simulated intensity vs. height curves neglecting actual roughness effects. Therefore, the measurements previously obtained are considered as preliminary results and are used here as starting points in some particular cases. This current project is focused on improving the surface roughness measurements through improved image analysis, surface roughness modeling, intensity computations, and, consequently, generating a simulated intensity vs. height curve where surface roughness effects are actually accounted for. In addition, improved particle size measurements are performed.

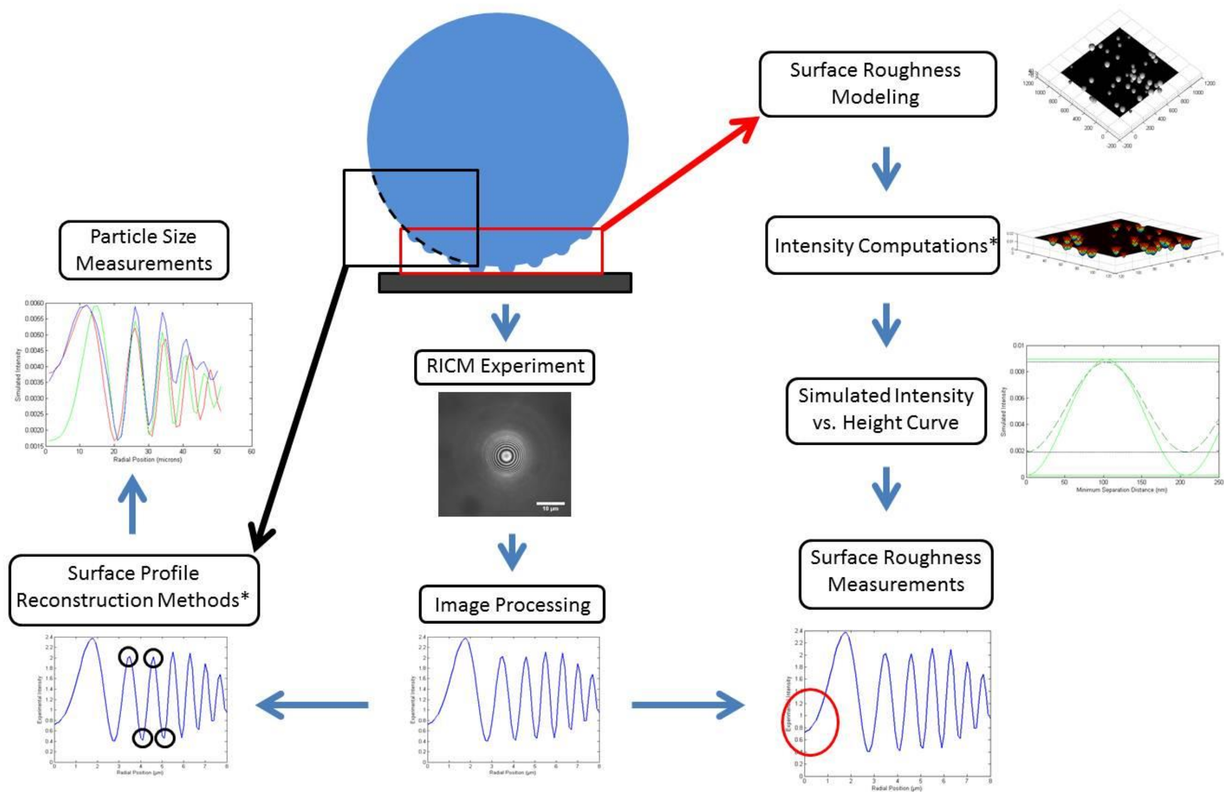

Figure 3. Methodology.

Image processing

Image processing is done using ImageJ with custom macros. The first step in the process is background homogenization, which uses the RICM images of the cover glass exposed to air without particles, in order to improve consistency and accuracy across multiple experiments. Then, a square selection is made around each individual particle's interferogram and the second macro located the center and obtains a circular average of intensities from the center at increasing radial distances. This is followed by a "zero" intensity subtraction (from the dark region outside the field of view), and normalization by exposure time.

Image processing was improved in the present work by optimizing a threshold value in the center finding routine. MATLAB was used to simulate intensity profiles corresponding to spherical particles ranging from 1-100 μm radius. For each size, a predetermined set of coordinates were selected that represented the center of the RICM interferogram with circular symmetry relative to the central pixel (Figure 4). The MATLAB program generates a pixelated RICM image (1 pixel = 100 x 100 nm square) that can then be analyzed using an ImageJ macro to determine the center of the interferogram using different threshold values, from 0.6 to 1 increasing at 0.01 increments. The coordinates for the center at different threshold values were compared to the actual values in order to determine which threshold value provides the most accurate center calculation in ImageJ. Another parameter that was considered was the level of "noise" in the RICM image, where the relative amount of noise added is a function of the intensities (Figure 4).

Surface roughness modeling

A MATLAB program provided by the Ugaz Research Group is used to simulate randomly dispersed asperities on a given planar area (typically a one micron square). The size of the asperities is of a normal distribution defined by an average size, standard deviation, and minimum and maximum (three standard deviations below and above the average, respectively) based on previous experimental results (5), and their shape is assumed to be hemispheres. The program generates randomly selected asperities from the given distribution and places them one by one on the predetermined area, allowing for partial overlapping between asperities, until a set surface coverage is achieved. As a result, surfaces covered with 0-90 % asperities have been obtained (Figure 5).

The maximum asperity size, which determines the closest distance the rough surface can be with another smooth planar surface, and the average elevation of the surface (m) are relevant parameters also computed for each rough surface generated. Other parameters that are commonly used to describe surface roughness measure the variation in height relative to a reference plane(12). The descriptors that were recorded in the simulations were the variance (σ^2) and Root Mean Square (RMS). Simulations were done with different parameters in order to determine sets of data that will encompass a large range of RMS and variance values. This ensures that the simulated intensity vs. height curves will be representative of a wide range of surface conditions.

$$(1)\ \sigma^2 = \frac{1}{LxLy}\int_0^{Lx}\int_0^{Ly}(z-m)^2\,dxdy$$

$$(2)\ m = \frac{1}{LxLy}\int_0^{Lx}\int_0^{Ly} z\,dxdy$$

$$(3)\ RMS^2 = \frac{1}{LxLy}\int_0^{Lx}\int_0^{Ly}(z)^2\,dxdy$$

Here z(x,y) represents the surface height, and Lx and Ly are the profile length, in the x and y direction respectively.

Roughness effects on intensity computations

Asperities in the order of tens of nanometers are smaller than the wavelength of monochromatic green light employed here; therefore, their detailed picture cannot be obtained because resolution issues come into play. However, the effects of these nanometer size features are expected to be present in the RICM images, especially in positions of the image plane where the particles are closer to the substrate (i.e. near the center of the interferograms) and, for quite large features, a few pixels with intensities that differentiate from their surroundings indicate their presence, as shown in Figure 6. Here it is considered that these effects on the intensities are mainly due to reflections from different planar parallel interfaces that are part of the asperities themselves;

consequently, the original hemispherical geometry assumed for the asperities is replaced by a series of three cylinders of decreasing diameter with the same size as the original asperity (Figure 6). This new geometry is used for computing intensities corresponding to rough surfaces by means of a modified RICM planar parallel interfaces image formation model that was implemented in a MATLAB program provided by the Ugaz Research Group.

Simulated intensity vs. height curve

From the simulations performed above, a simulated intensity vs. height curve can be generated (Figure 3). Using this curve, surface roughness measurements can be obtained from experimental data. Intensities corresponding to different separation distance values (heights) between the rough surface and a planar parallel smooth substrate are simulated; the resulting intensities simulated on a specified area are then averaged over 100 x 100 nm squares using the trapezoidal rule to replicate the effects of pixels found in a typical RICM image. The next step is to take the matrix of pixels and find the average intensity around a certain coordinate, which represents the center of a RICM interferogram with circular symmetry. Given an input of the x and y coordinate, the average intensity of a 100 x 100 nm square is calculated around the specified point (i.e. the intensity of the central pixel). This intensity of the central pixel varies depending on the x and y coordinate so 400 intensity simulations were performed to accurately model one scenario. The different scenarios account for the statistical distribution of the asperity sizes, the surface coverage, the refractive index of the particle, and the separation distance value (height) between the rough surface and a planar parallel smooth substrate. The intensity simulations provide data that reflects the range of intensity values expected at a particular separation distance. From this information an average intensity vs. height curve can be obtained.

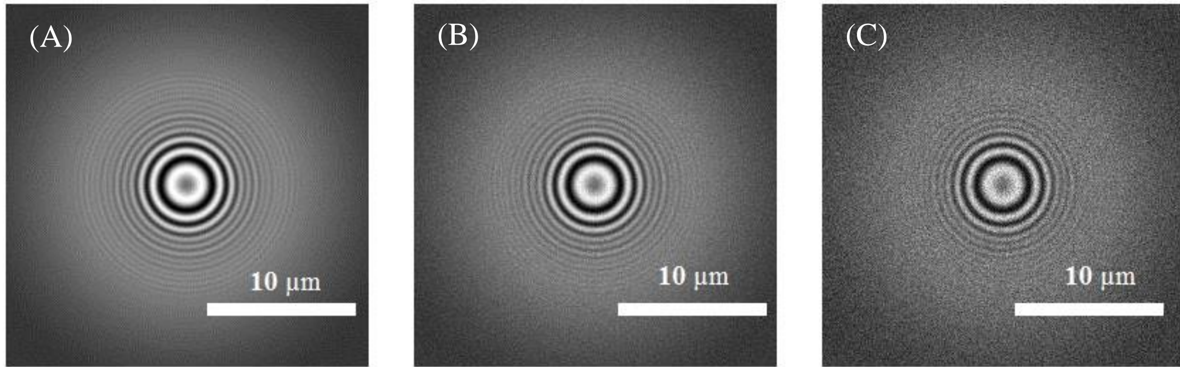

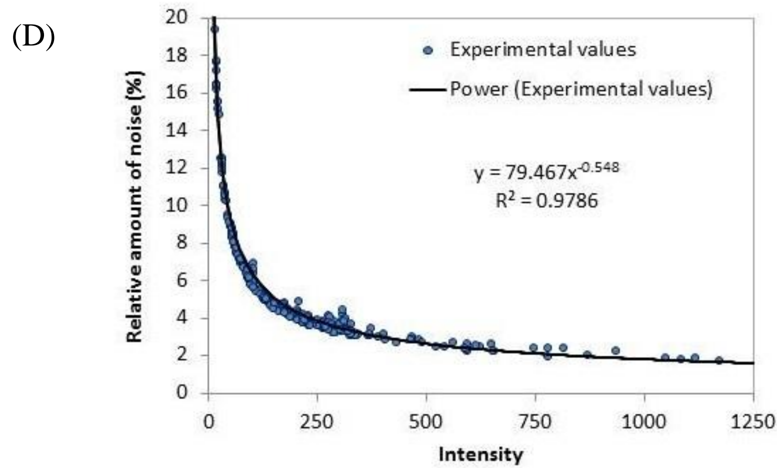

Figure 4. Simulated RICM images generated by MATLAB. The simulated particles are 10 µm radius spheres located 50 nm above the substrate. (A) Image without noise and maximum intensity of 4095. (B) Image with a normal amount of noise and maximum intensity of 1500. (C) Image with high amount of noise and maximum intensity of 150. Maximum intensity based on a 12 bit gray scale. (D) Correlation used for adding noise to interferograms. (E) 1 μm^2 selections around the central region of two RICM interferograms exhibiting different coordinates for the center (white circle) relative to the central pixel (black). Notice the differences in the pixel patterns.

10 % : Number of asperities = 27; Max = 57.9 nm; Average elevation = 2.7 nm; ; σ = 8.2 nm; RMS = 8.5 nm

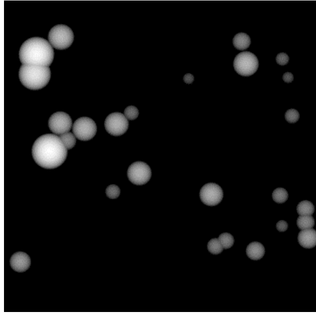

50 % : Number of asperities = 185 ; Max = 59.9 nm; Average elevation = 13.9 nm; σ = 14.1 nm; RMS = 18.6 nm

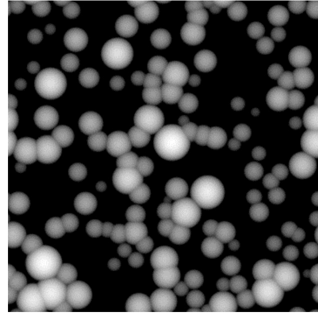

90 %: Number of asperities = 445; Max = 60 nm; Average elevation = 26.5 nm; σ = 11.6 nm; RMS = 26.1 nm

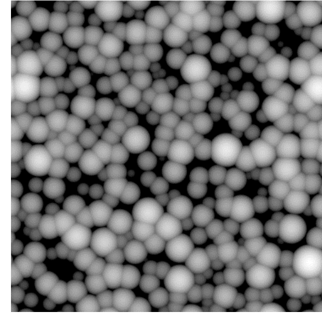

Figure 5. Illustration of simulated asperities, showing different amounts of surface coverage over a 1x1 micron square. Black = Zero elevation; White = Maximum elevation. Asperity size distribution: Average = 30 nm; standard deviation = 10 nm; minimum = 1 nm; maximum = 60 nm

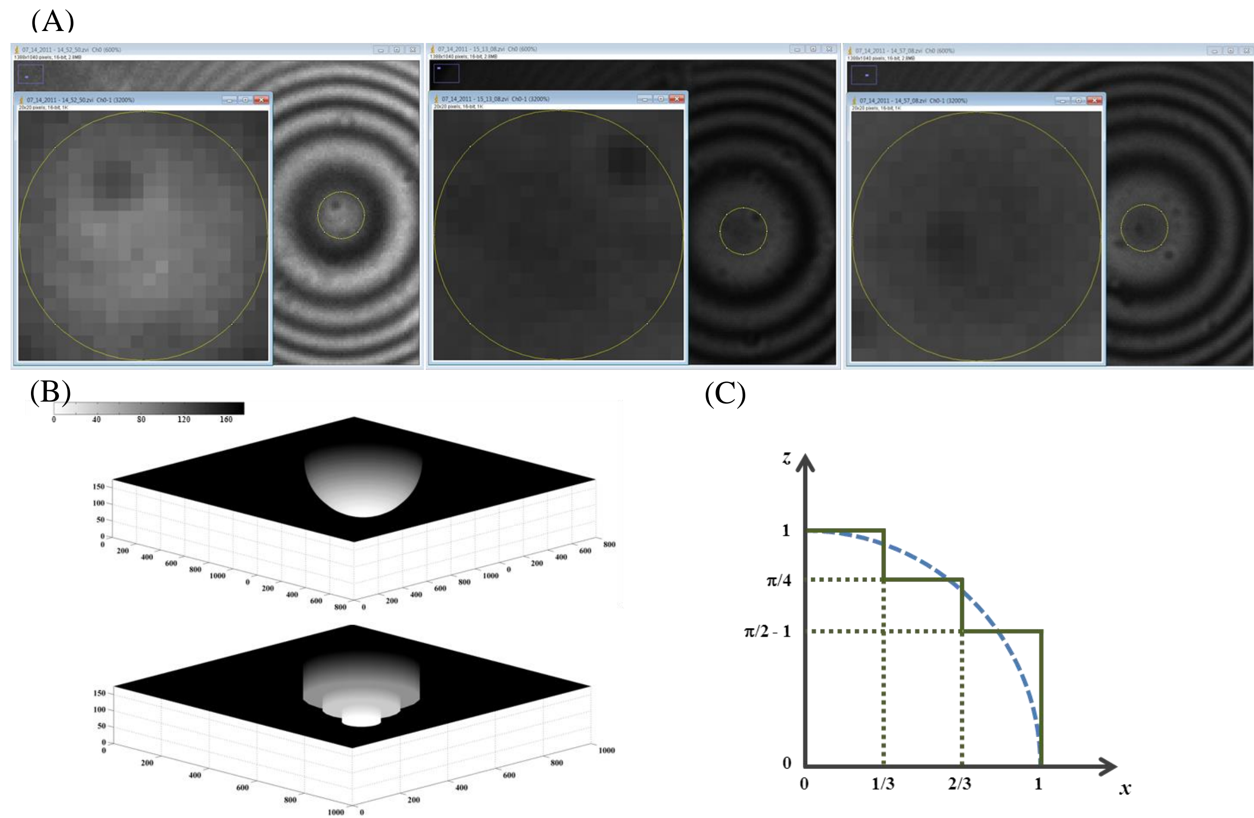

Figure 6. (A) Shows how asperities are visually indicated on the RICM images using 2 μm diameter circular selections on images from Glass 30-50 in 0.1 M NaCl solution. (B) Illustration of the geometrical model used for the asperities. (C) Shows how the spherical geometry can be reduced to the cylindrical geometry.

Statistical methods

The distribution of asperity sizes used in the simulations are fitted to a Gaussian distribution, which was the type of distribution observed in experimental measurements of the surface roughness (5). The Gaussian probability density function (PDF) for a random variable x is defined by the following formula:

$$(4)\ PDF(x) = \frac{1}{\sigma\sqrt{2\pi}} e^{-\frac{(x-\mu)^2}{2\sigma^2}},$$

on the domain $[-\infty, \infty]$, where σ is the standard deviation, σ^2 is the variance, and μ is the mean. Integrating the PDF between $a \leq x \leq b$ gives the probability for x to take a value in this particular in. Therefore, the cumulative distribution function (CDF) for the Gaussian distribution is:

$$(5)\ \mathrm{CDF}(h) = \mathrm{Probability}(x \leq h) = \frac{1}{2}\left[1 + erf\left(\frac{x-\mu}{\sigma\sqrt{2}}\right)\right],$$

where *erf* is the error function. The CDF describes the probability that x will be less than or equal to a particular value h. Notice that the distribution is normalized since $\mathrm{CDF}(\infty) = 1$.

The beta distribution was used to describe the calculation error in the center pixel value. The beta distribution has a domain of [0, 1] and is described by two shape parameters, $\alpha, \beta > 0$ (13). The PDF of the beta distribution is:

$$(6)\ PDF(x) = \frac{x^{\alpha-1}(1-x)^{\beta-1}}{B(\alpha,\beta)},$$

where $B(\alpha, \beta)$ is a normalization constant, and its CDF is given by:

$$(7)\ CDF(h) = \mathrm{Probability}(x \leq h) = \sum_{j=a}^{\alpha+\beta-1} \frac{(\alpha+\beta-1)!}{j!(\alpha+\beta-1-j)!} h^j (1-h)^{\alpha+\beta-1-j}$$

The mean and variance for the beta distribution are given by:

$$(8)\ \mu = \frac{\alpha}{\alpha+\beta}$$

$$(9)\ \sigma^2 = \frac{\alpha\beta}{(\alpha+\beta)^2(\alpha+\beta+1)}$$

CHAPTER III

RESULTS

Image processing improvements

Center measurements of the simulated RICM interferograms were performed in ImageJ and compared to the actual center values set in a regularly spaced grid inside the central pixel. The average and maximum error of the center calculation was compared for the different threshold values as well as for the different particle sizes with different amounts of intensity noise. For most particle sizes, the error vs. threshold value curve exhibited a sinusoidal behavior, up to a certain threshold value (cut-off threshold), and then the error leveled off as shown in Figure 7. Notice that the error is presented in pixel units (1 pixel = 100 nm), so sub-pixel resolution for the center measurement can only be guaranteed at thresholds larger than the cut-off value. As particle size increased, the cut-off threshold value also increased to a maximum of around 0.87 for the case of a 7 μm radius particle. For particles larger than 7 μm, the cut-off threshold value began to decrease, and for particles greater than 50 μm in radius, there was little difference in error for the different threshold values studied (Figure 7c).

For a given particle size and for each threshold value, only the maximum error and the maximum average of the error among all noise conditions are considered for further computations. Figure 8 shows the average and maximum error calculated from the ensemble of all the particle sizes with respect to the threshold value. The minimum average error is 6.49 nm with a standard deviation of 4.7 nm at a threshold value of 0.91. The lowest maximum error (21.21 nm) is obtained at a

threshold value of 0.92 (7.25 nm average error with a standard deviation of 4.8 nm) which is selected as the optimum value for the center finding measurement.

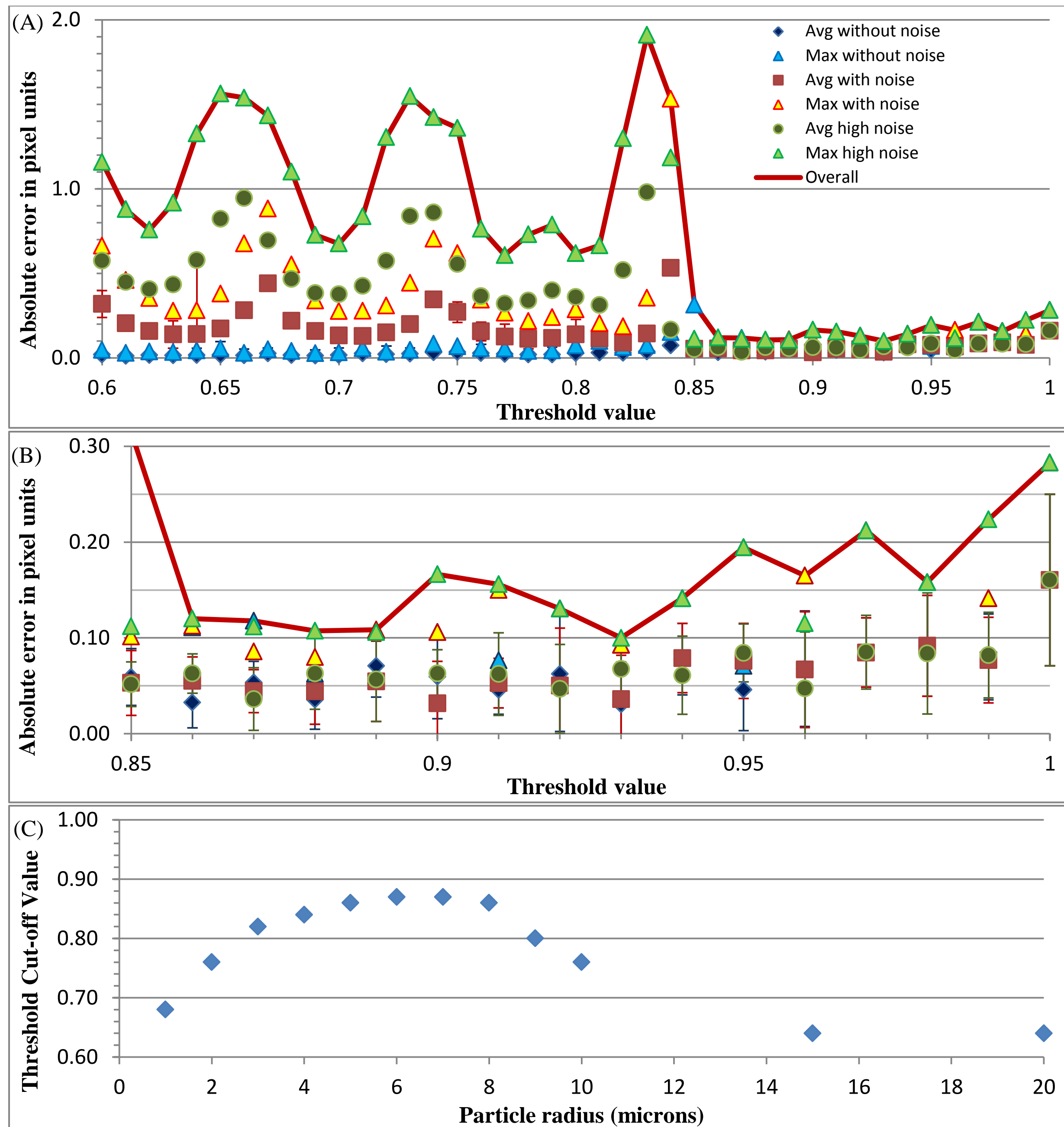

Figure 7. Center calculation error for a simulation of a 5 µm radius particle. (A) Shows how the error changes depending on the threshold value used for the center calculation. For this case, threshold cut-off is around 0.86. (B) Zoom in on the area of the plot where the error has flattened out. (C) Shows how the threshold cut-off value changes with particle size.

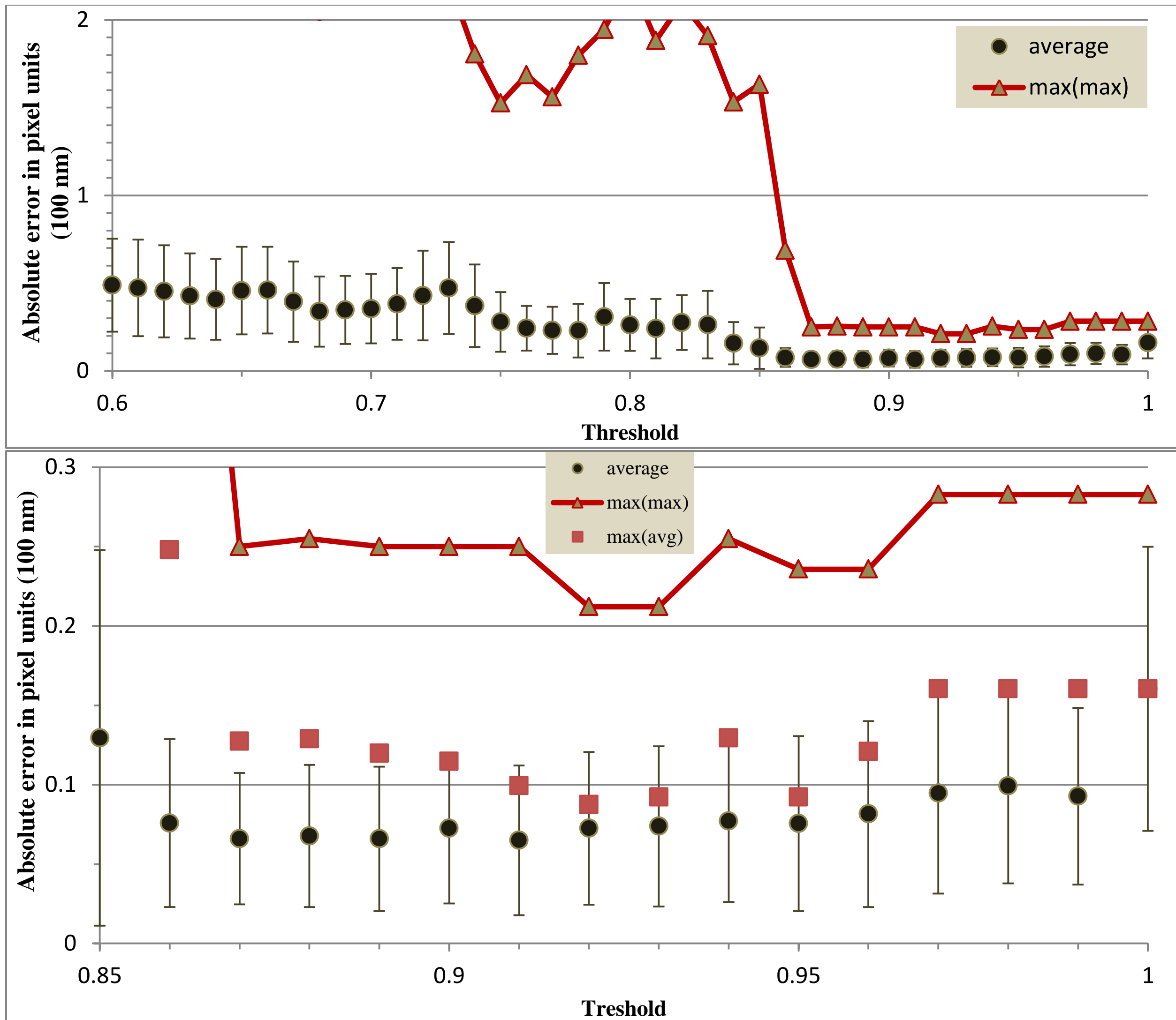

Figure 8. Ensemble of the average and maximum error of all particle sizes simulated as a function of the threshold value.

Implementing the optimized threshold value in the center finding routine reduces the error especially in cases where there is noise in the image (Figure 7). Experimentally, images present different levels of noise depending on the exposure time, so the accuracy of center measurements on experimental data will improve significantly for dynamic studies that require the exposure time to be reduced to a minimum leading to highly noisy images.

The next step was to quantify the distribution of error in the center calculations. The center calculation error was measured for 999 simulations of 10 μm radius particles with randomly generated center coordinates. This was repeated for simulations with no noise, regular noise, and high noise. A probability density and cumulative distribution function of the normalized error and the frequency was plotted for each scenario (Figure 9 and 10). Because the error is a random variable limited to a finite interval, a beta distribution was fitted to the cumulative distribution of the error using MATLAB to solve the nonlinear least-squares fitting (the error is normalized to the maximum error so the domain of the normalized error is [0, 1]). The curve fitting in Figure 10 shows that the beta distribution successfully models the behavior of the error resulting from different noise conditions. Different parameters associated with the probability distribution function are listed in Table 2. Finally, the differences in the error measurements between the particles without noise and the particles with high noise were statistically significant according to the t-test at a 90% confidence interval. As seen in Figure 9, the probability density of the error for both the regular noise and high noise images are similar. This suggests that the center analysis technique that is being implemented here is robust enough to be suitable for a range of possible scenarios that may be encountered experimentally.

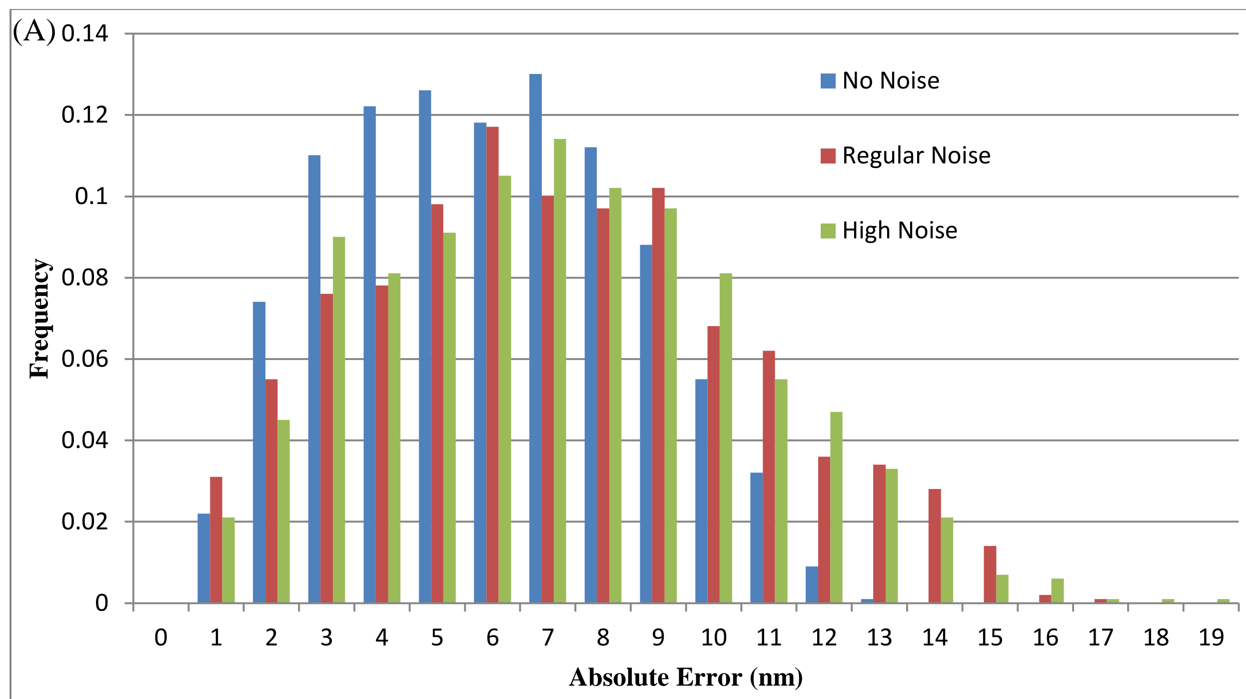

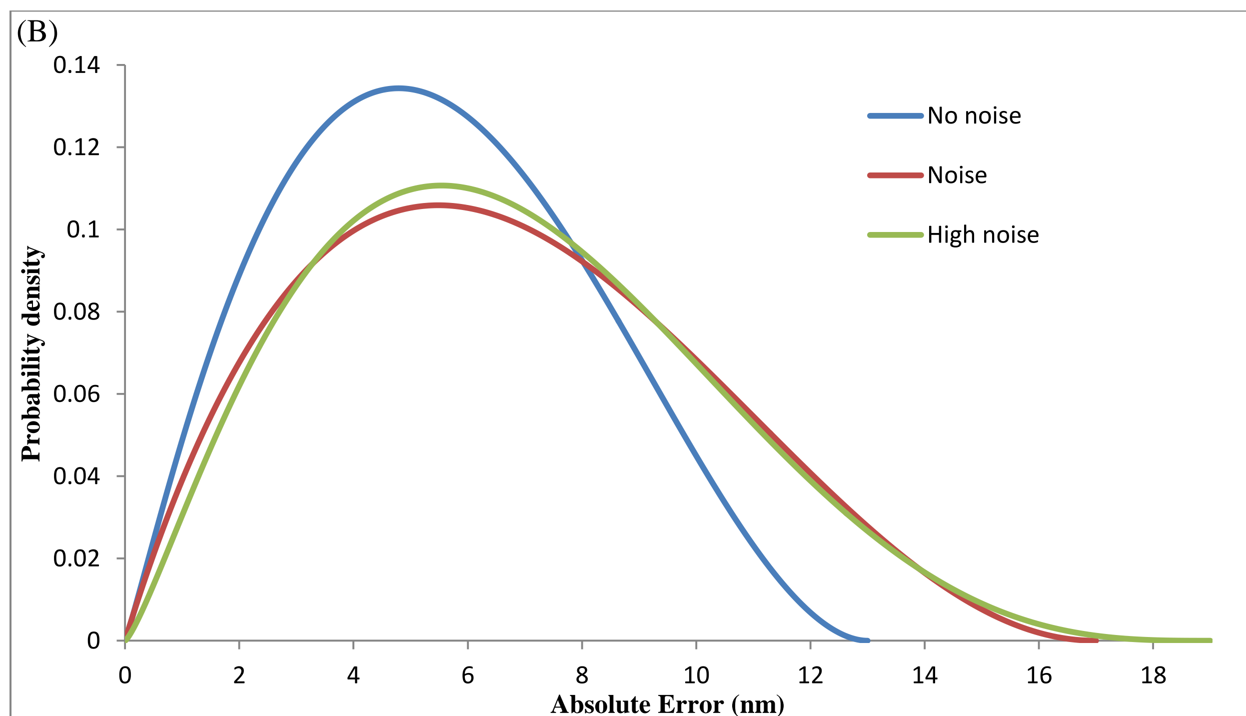

Figure 9. Simulation of 10 µm particles (sample size 999) with randomly generated center coordinate. (A) Histogram of the error in the center calculation. (B) Probability density function fitted to the data

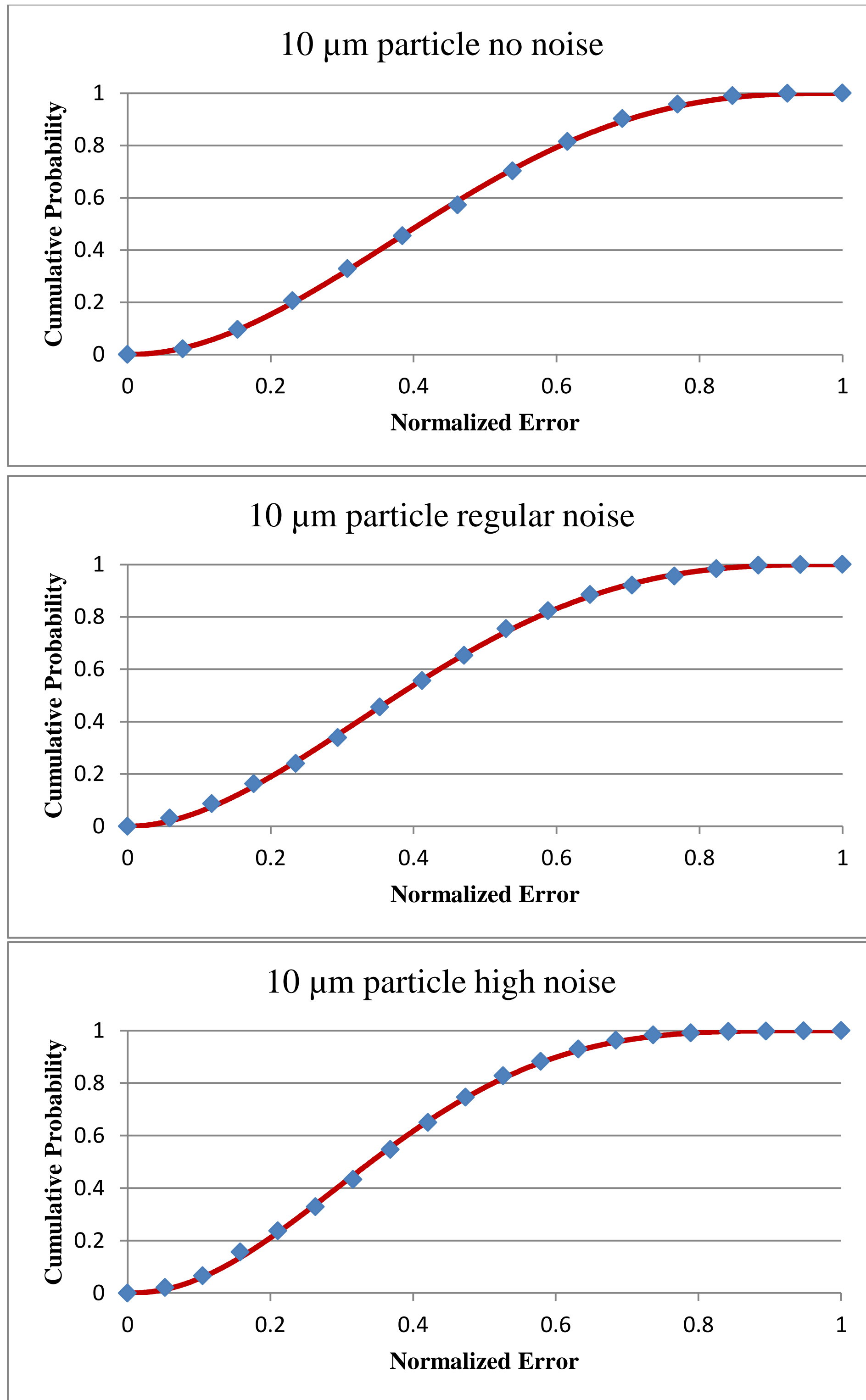

Figure 10. Cumulative distribution function of the simulations of 10 μm particles with randomly generated center values. Blue dots are data. Red line is the beta distribution, best fit curve.

Table 2. Summary of relevant parameters of the error calculations for the simulations of interferograms from 10 μm particles with randomly generated centers.

	No noise	Noise	High noise
Based on normalized error			
Alpha	2.1064	1.9861	2.2831
Beta	2.8961	3.0696	4.1163
Mean	0.421069	0.392844	0.356768
Variance	0.040611	0.039387	0.031014
Without error normalization			
Min (nm)	0	0	0
Max (nm)	13	17	19
Mean (nm)	5.47	6.68	6.78

Characterization of surface roughness simulations

The surface roughness modeling program also calculates some common parameters that describe the simulated rough surface, including the average surface height (m), the standard deviation of surface heights (σ), and the Root Mean Square (RMS). These parameters were recorded for the different systems that were used for the development of the simulated intensity vs. height curve. Also, surface roughness simulations were performed to determine the effects of different parameters, including asperity size, standard deviation of asperity size, surface coverage, and repeated simulations, on the different surface roughness parameters. For instance, Table 3 shows the effect of increasing surface coverage (for the same asperity distribution) after repeated simulations were performed, where repeated simulations for the same inputs (mean, standard deviation, minimum, maximum, and % surface coverage) account for variability in the results. Table 4 presents the effect of increasing the average asperity size (at constant surface coverage), and it can be seen that increased variability in the results is due to fewer asperities in the simulated region as asperity size increases.

Table 3. Statistics from 20 simulations comparing the effect of surface coverage on surface roughness using the same statistical distribution of asperity sizes (mean 30 nm, standard deviation 6 nm, minimum 12 nm, maximum 48 nm)

sc (%)	*m* Mean ± Std Dev	σ Mean ± Std Dev	RMS Mean ± Std Dev	Average Number of Asperities
5	1.05 ± 2.40	4.96 ± 1.70	5.06 ± 2.07	17.6
25	5.46 ± 1.30	10.38 ± 2.22	11.73 ± 0.89	89.8
50	11.18 ± 0.19	12.66 ± 0.18	16.89 ± 0.23	192
75	17.41 ± 0.19	12.26 ± 0.14	21.29 ± 0.23	317.1
90	21.56 ± 0.29	10.24 ± 0.18	23.87 ± 0.27	434.4

Table 4. Statistics from 20 simulations for different asperity size distributions. Standard deviation at 20% of mean asperity size, minimum = mean – 3*std. dev, maximum = mean + 3*std. dev. 5% surface coverage.

Avg. Asperity Size (nm)	*m* Mean ± Std Dev	σ Mean ± Std Dev	RMS Mean ± Std Dev	Average Number of Asperities
30	1.08 ± 0.06	5.10 ± 0.27	5.21 ± 0.28	16.95
50	1.74 ± 0.18	8.29 ± 0.86	8.47 ± 0.88	6.35
75	2.48 ± 0.33	11.97 ± 1.45	12.22 ± 1.48	2.8
100	2.86 ± 0.52	14.33 ± 2.32	14.62 ± 2.37	1.6

The simultaneous effects of the percent surface coverage and the asperity size on the surface roughness parameters can also be studied (Figure 11). The standard deviation was set at 20% of the mean asperity size and the minimum and maximum were ± 3*standard deviation. A series of linear trends (with increasing slopes as asperity size becomes larger) are obtained when the average surface height and RMS are plotted as a function of surface coverage and the asperity size is used as a parameter. A quadratic function can be fitted to the standard deviation vs. surface coverage plot revealing that for a single asperity size distribution it is possible to have the same surface standard deviation using two different surface coverage values. Another set of simulations focused on the effect of the standard deviation of the asperity distribution (Figure 12). For these, the standard deviation changed based on the coefficient of variance (standard deviation divided by the mean) and the surface coverage was set at 25%. In general, a somewhat linear increase of the surface descriptors is observed as the coefficient of variance of the asperity distribution increases.

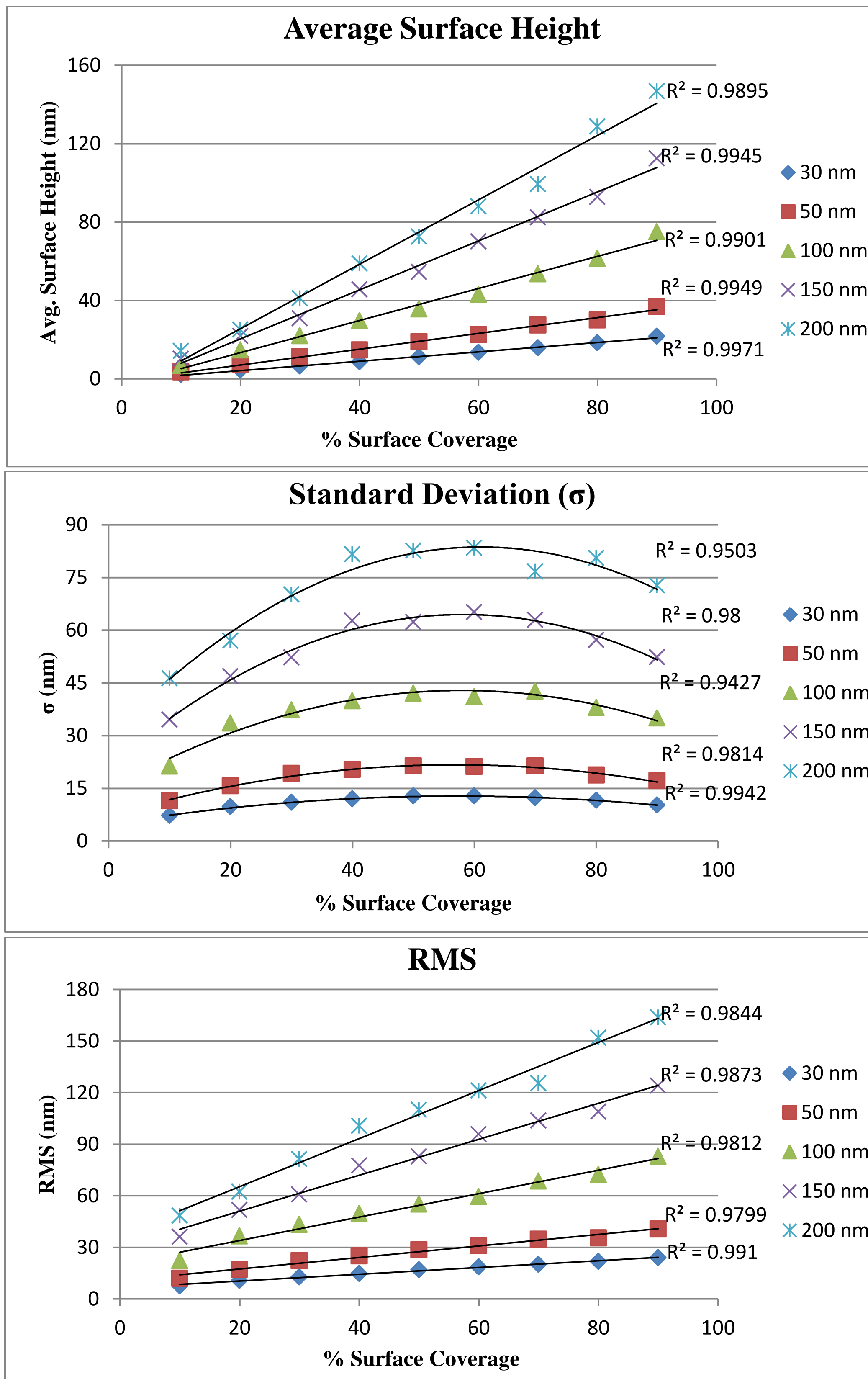

Figure 11. Plot comparing the effect of percentage surface coverage on the average surface height, standard deviation (σ), and the Root Mean Square.

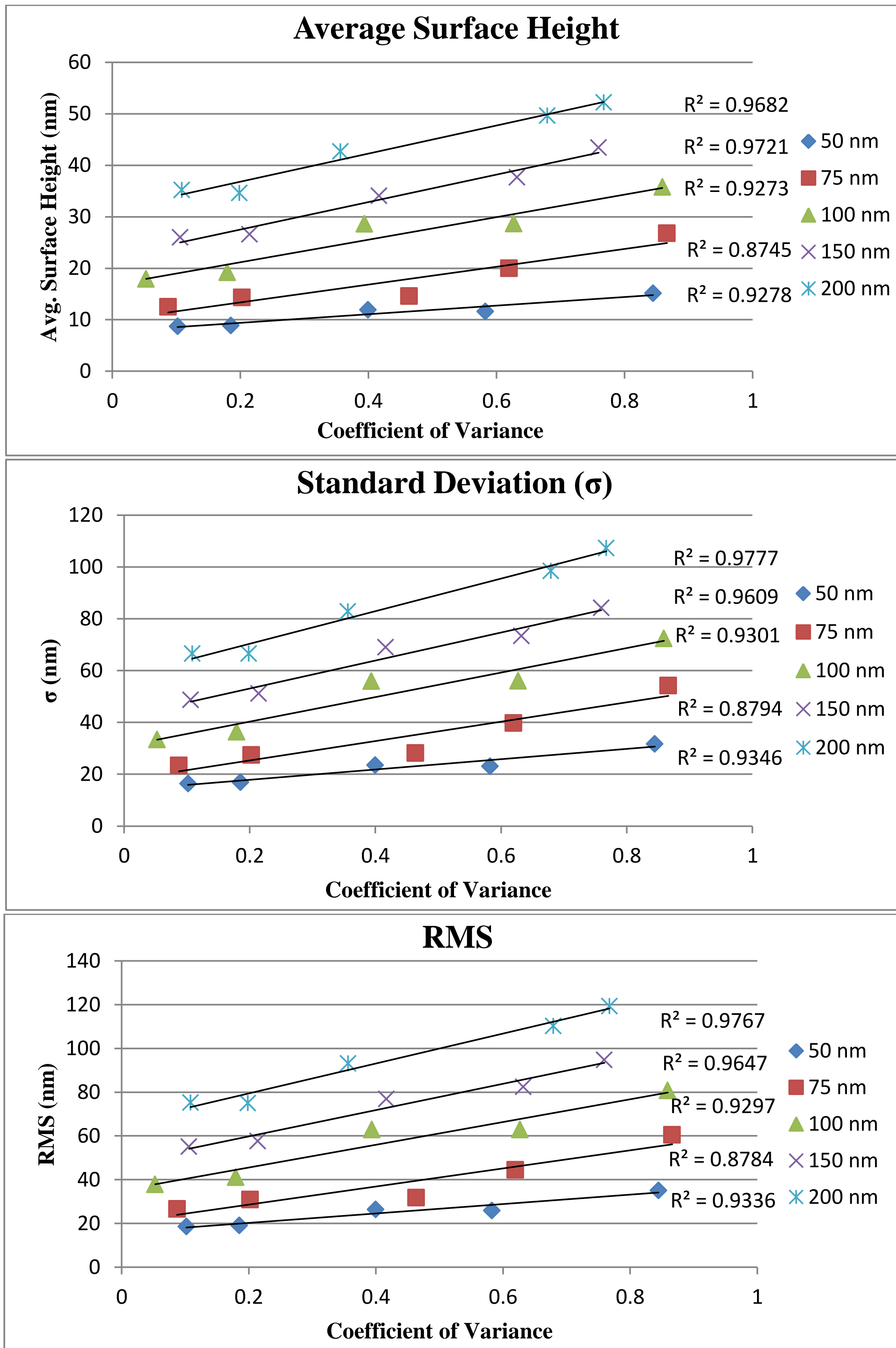

Figure 12. Plot comparing the effect of standard deviation of the asperity size distribution on the average surface height, standard deviation (σ), and the Root Mean Square. The x-axis is scaled to the measured coefficient of variance (standard deviation divided by the mean asperity size)

Simulated intensity vs. height curves

Here, the closest region of the spherical particle with the substrate is approximated using a planar surface for both smooth and rough particles. This geometric approximation (that becomes more accurate as particle size increases) allows simulated intensity vs. height curves to be generated for different particle and surface conditions, see Table 5.

Table 5. Ensemble of systems used for roughness measurements. n_0 is the refractive index of the planar substrate the particle is placed on. n_1 is the refractive index of the medium (water). n_2 is the refractive index of the particle. INA = 0.48; NA = 1.25

Single layer systems		
n_0	n_1	n_2
1.53	1.333	1.51 1.59

Initially, computations were performed for surface coverage of 5 %, 15 %, 25 %, and 35 % for each one of the following formulations (asperity distributions in nm):

1. For monodisperse samples of PSL 15 µm and Glass 15 µm diameter beads (n_2=1.59):
    - Asperity distributions: [30 ± 6], [30 ± 7.5], [30 ± 9], [30 ± 10.5], and [30 ± 12]
2. For polydisperse Glass beads 10-30 µm diameter (n_2=1.51):
    - Asperity distribution: [35 ± 15]
3. For polydisperse Glass beads 30-50 µm diameter (n_2=1.51):
    - Asperity distribution: [55 ± 15]

A few observations can be made from these simulations. In general, at low surface coverage values, the curve for the rough particle is similar to the curve for a smooth particle. At higher surface coverage values or larger asperities, there is a noticeable difference between the

simulated intensities for the rough particle compared to the simulated intensities for the smooth particle. The difference between the intensity vs. height curve of the rough particle and smooth particle can be related to their visibility, which is a function of the maximum and minimum intensity value (Equation 10), as computed from the first peak and valley, respectively.

$$(10)\ Visibility = \frac{I_{max} - I_{min}}{I_{max} + I_{min}}$$

For instance, Figure 13 illustrates the effect of surface roughness on the visibility. There are some key features to notice when comparing the two plots showing the difference between a smooth sphere (orange line) and a sphere with surface roughness (blue line). The gap (circled in red) between the two curves changes depending on the amount and size of the asperities on the particle. This difference can be quantified using the relative visibility (the ratio between the visibilities of the rough and smooth particles). Another important observation from Figure 13 is that at 35% surface coverage there is a very low probability of finding a 300 x 300 nm square area smooth enough to be closer than 20 nm or less to the substrate (circled in green).

As it became clear that the relative visibility was an important parameter sensitive to roughness, the next step was to determine which surface descriptor is more strongly correlated to the relative visibility. From the equations of the best fit lines for the different surface parameters, different formulations can be simulated that would yield the same value for the surface parameter. For example, a standard deviation of 35 nm can be obtained from an average asperity size of 100 nm and either 88.7% or 27.3% surface coverage (Table 6). Two different formulations were found that would result in the same value for the standard deviation of the surface roughness, as summarized in Table 6. Intensity vs. height curves were generated for all the formulations to determine the relative visibility. From these results, it can be seen that out of the three surface

parameters calculated (average surface height, standard deviation, and RMS) both the average surface height and the RMS changed despite the fact that the relative visibility was the same, and the standard deviation has the strongest correlation to the relative visibility.

The relative visibility of interference fringes is commonly related to the standard deviation of the surface roughness (Equation 1). Figure 14 plots several equations that Atkinson et al. reported as relationships for visibility and the standard deviation (σ) of the surface roughness, in their review of optical interferometry (14). The data obtained from the simulations seems to agree with some of the previously reported equations. Previous experiments were performed to measure the particle size and minimum separation distance from RICM images, but did not account for the roughness effects (5). With the new simulated intensity vs. height curves that account for the effects of roughness, more accurate results can be obtained.

Additional simulations were performed to calculate the intensity for heights from 260-550 nm (Figure 15). Comparing the relative visibility of different intensity extrema showed consistent visibility throughout the intensity vs. height curve. The first peak compared to the first valley had a relative visibility of 0.8216, the second peak compared to the first valley had a relative visibility of 0.8214, the second peak compared to the second valley had a relative visibility of 0.818, and the third peak compared to the second valley 0.816. These results show that the standard deviation of the surface can also be determined from the relative visibility (Figure 14) of higher fringe orders, which is a significant finding because when asperities become larger (>100 nm), the first peak will be distorted and eventually won't be measurable. Figure 16 compares the maximum and minimum simulated intensity at a given height. The results show

that the range of possible simulated intensity values for a given height decreases as the height increases, in other words, the effect of the asperities in the variability of the intensities is somewhat smoothed out.

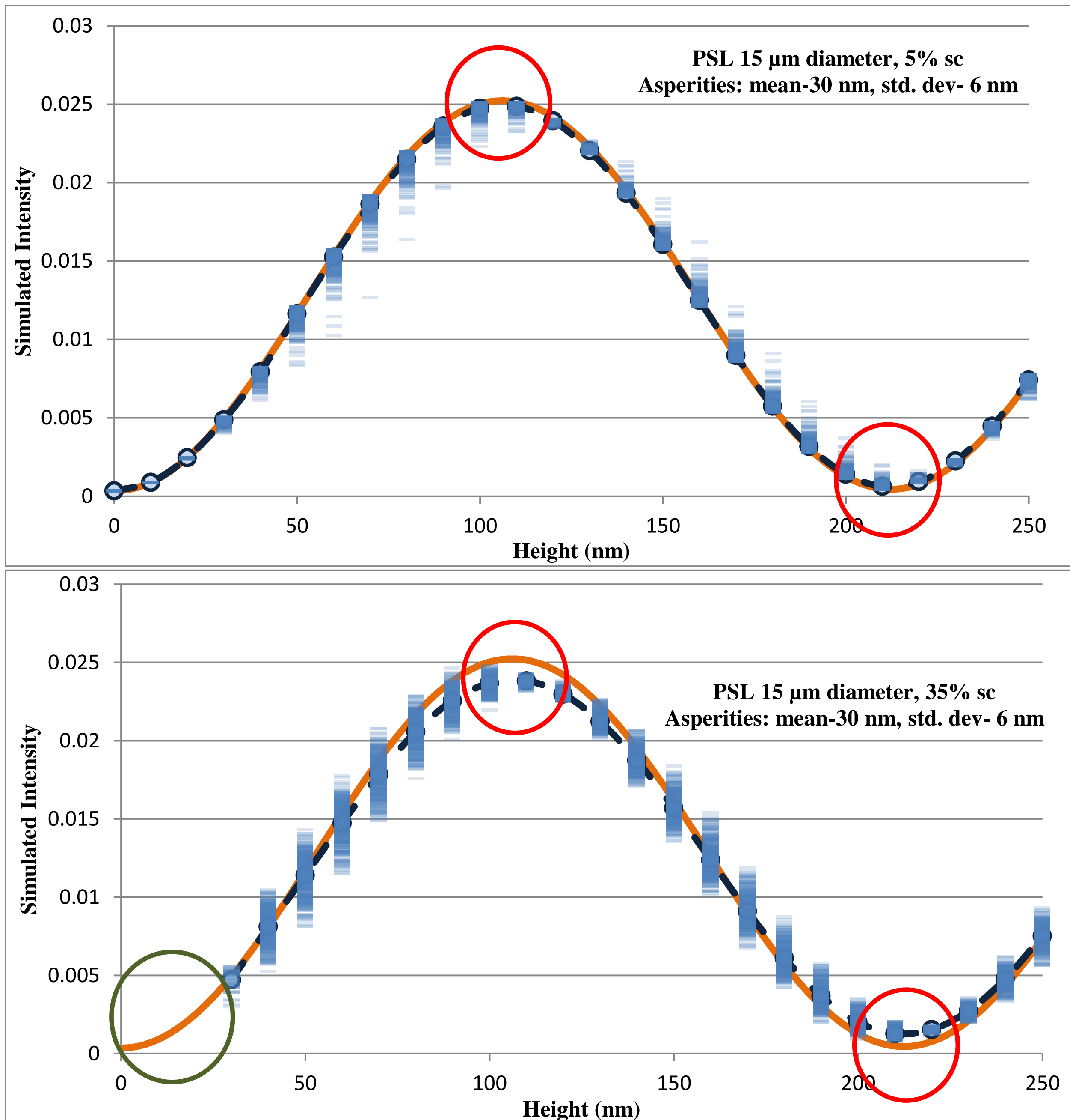

Figure 13. The orange line is the simulated intensity vs. height curve of a smooth spherical particle. The blue data represents the simulated intensity of rough particles.

Table 6. Summary of formulations simulated to determine strongest correlation between different surface parameters and relative visibility. Standard deviation of asperity size distribution set at 20 % of mean asperity size.

σ (nm)	Mean Asperity Size (nm)	% SC	m (nm)	**Actual σ (nm)**	RMS (nm)	**Relative Visibility**
35	100	88.7	71.21	**35.38**	79.52	**0.65**
35	100	27.3	20.00	**35.87**	41.07	**0.62**
30	75	80.0	48.01	**30.45**	56.85	**0.71**
30	75	30.0	16.34	**27.38**	31.88	**0.68**
20	50	76.4	30.07	**20.46**	36.37	**0.84**
20	50	37.4	13.95	**20.15**	24.51	**0.82**
15	40	80.0	24.82	**15.64**	29.33	**0.90**
15	40	25.0	6.98	**13.26**	14.98	**0.91**
11	30	90.0	21.22	**10.05**	23.48	**0.93**
11	30	20.0	4.31	**9.42**	10.36	**0.94**

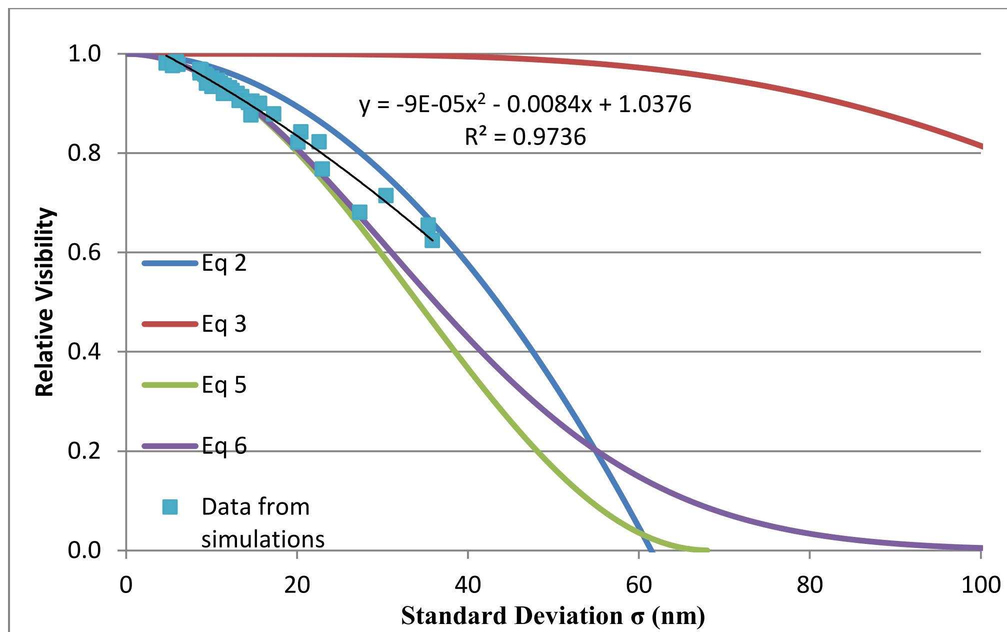

Figure 14. Comparison of data from simulations with equations reported in previous literature. The equation numbers correspond to the equations listed in Atkinson's review of optical interferometry (1980).

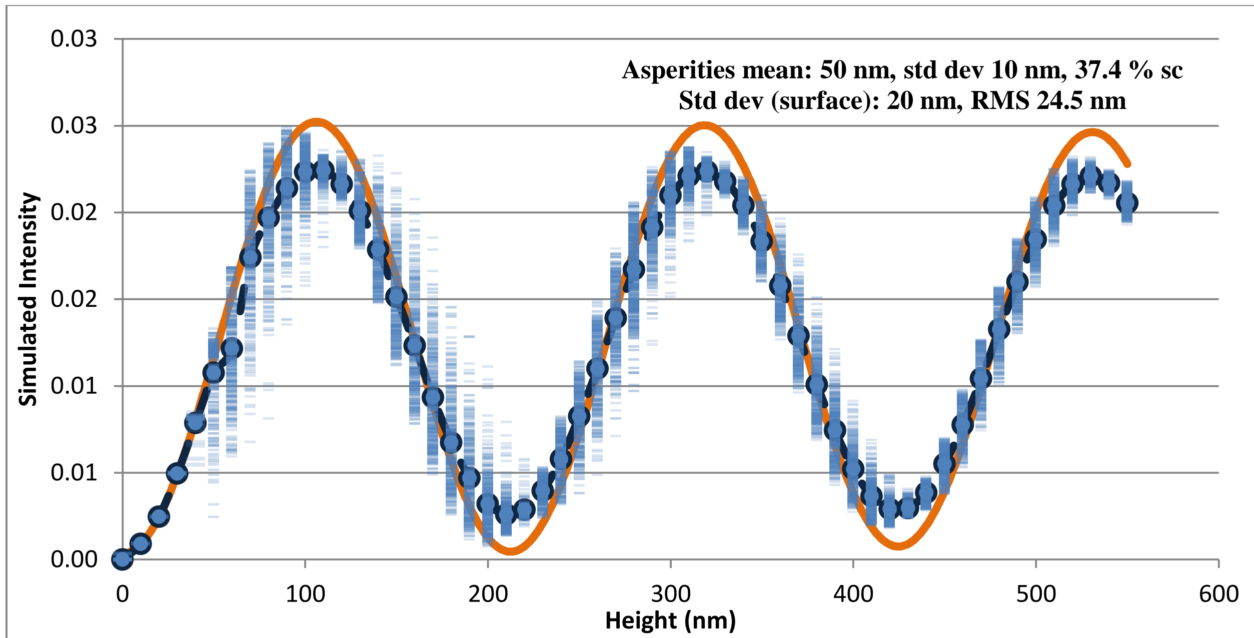

Figure 15. The orange line is the simulated intensity vs. height curve of a smooth spherical particle. The blue data represents the simulated intensity of rough particles. Higher fringe orders can be used to measure the visibility of peaks and valleys when asperity size increases and the first fringe is highly distorted.

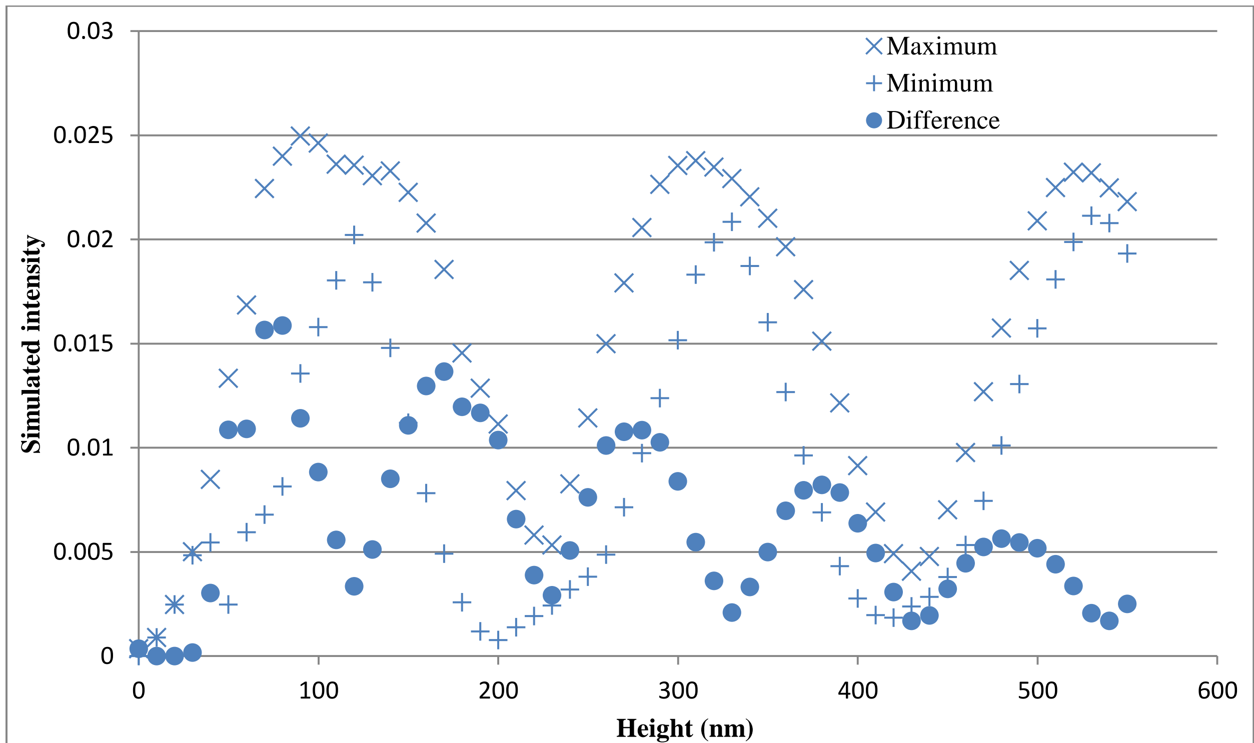

Figure 16. Comparison of maximum and minimum simulated intensity for a given height.

Particle size and minimum separation distance measurements

Recalculations of the particle size and minimum separation distance measurements of the previously collected experimental RICM data (5) were performed. The improvements made were based on the better understanding of the effects of surface roughness on the intensity vs. height curve (Figure 13). These new particle size and MSD measurements are shown in Table 7. For the monodisperse samples, the particle size measurements can be compared to the manufacturer's values. The RICM measurements gives an average diameter of 15.04 µm and a coefficient of variation of 14.1% compared to the manufacturer's values of 15 µm and 14%, respectively. For the glass beads, the expected diameter is 15 µm and the RICM measurement gives an average diameter of 15.78 µm. These results are closer to the manufacturer's information compared to the RICM measurements done previously (5), which shows the importance of accurately accounting for surface roughness.

Table 7. Summary of particle size and MSD measurements.

Particle (sample size)	**Radius (µm) Mean ± Std Dev**	**MSD (nm) Mean ± Std Dev**	**Visibility Mean ± Std Dev**	**σ (nm) Mean ± Std Dev**
PSL 15 (192)	7.52 ± 1.03	41.0 ± 4.04	0.71 ± 0.04	29.28 ± 2.86
Glass 15 (121)	7.89 ± 1.21	40.2 ± 7.49	0.72 ± 0.05	28.77 ± 3.80
Glass 10-30 (181)	15.6 ± 3.54	44.1 ± 10.1	0.72 ± 0.08	28.52 ± 5.42
Glass 30-50 (128)	19.2 ± 5.21	59.8 ± 12.8	0.71 ± 0.14	28.83 ± 8.61

Comparing the two monodisperse samples both with expected diameters of 15 µm, it is interesting to see similar average MSD, visibility, and surface height standard deviation. The standard deviation for the MSD is higher for the Glass 15 samples compared to the MSD standard deviation of the PSL 15 samples, and that seems to correspond to the higher standard deviation for the surface height standard deviation (σ) as well. This comparison shows that

although the average surface roughness is similar for both samples, the distribution of the surface asperity sizes is different.

Now, comparing the polydisperse samples, the average MSD value for the Glass 30-50 sample is about 15 nm larger than that of the Glass 10-30 sample, which indicates larger asperities. The key difference in the visibility and σ between the two samples is seen in the standard deviation. Both samples have similar average visibility and average σ values, but the Glass 30-50 sample has a larger standard deviation for both values. In general, RICM is able to calculate particle size for both monodisperse and polydisperse samples. Also, the type of material does not affect the measurements.

CHAPTER IV

CONCLUSION

The goal of this study was to improve the methodology that is used for RICM image analysis of particle size and surface roughness. The first step was to improve the image processing technique by determining the optimal threshold value to reduce errors in the center pixel determination for a wide range of particle sizes and noise levels in the RICM image. It is found that an optimum threshold value of 0.92 guarantees sub-pixel resolution with an error of about 7 nm when finding the center of an interferogram with circular symmetry. The next step was to perform surface roughness modeling to determine the effects of surface roughness on the RICM measurements of particle size and surface roughness. The visibility (Equation 10) is the key parameter influenced by surface roughness. This information was used to recalculate the size and particle roughness from RICM images of monodisperse samples of polystyrene latex, and monodisperse and polydisperse samples of glass beads. The new measurements agreed well with the manufacturer's data and are an improvement over the previous calculations (5). Another important discovery is the ability to attribute the relative visibility of the interferogram to the standard deviation of the surface roughness (Figure 14), in agreement with previous correlations obtained for different interference setups. One application of this could be in a quality control setting, where the surface roughness needs to fit a certain range. RICM can be used to quickly determine the standard deviation of the surface roughness simply by measuring the visibility of the inteferogram.

The improved accuracy of the RICM calculations makes RICM a promising alternative to more popular microscopy techniques including the ones listed in Table 1. One key advantage of RICM is the unique ability to analyze individual particles from the bottom so that in situ and simultaneous characterization of both particle size and surface roughness can be performed. On the other hand, if statistics representing a sample of particles are desired, RICM has the ability to obtain information from large sample sizes (~300 particles), and can be used for both monodisperse and polydisperse samples. In the present study, RICM measured particles in the size range of 10-58 μm diameter, which is comparable to the other methods listed in Table 1 (2). Some possible applications include studying the effects on the adhesion of particles to a flat substrate in different deposition scenarios to improve existing adhesion and resuspension models. The sample preparation is also quick and can be prepared with different mediums, which can aid in the study of the different deposition scenarios.

One important future study would be to measure the surface roughness of the samples tested using another method to compare to the RICM measurements. Additional simulations can also be done to improve the accuracy of the visibility vs. standard deviation curve (Figure 14), especially to obtain data at higher values of standard deviation. Another consideration is to perform RICM measurements of particles that are larger or smaller, because the samples studied still are not close to the limit for RICM, estimated to be around 1-1000 μm diameter (2). So it would be interesting to see what modifications, if any, need to be done for the analysis of larger or smaller particles.

REFERENCES

1. Hu, S.; Kim, T. H.; Park, J. G.; Busnaina, A. A., Effect of Different Deposition Mediums on the Adhesion and Removal of Particles. *Journal of The Electrochemical Society* **2010,** *157* (6), H662-H665.

2. Limozin, L.; Sengupta, K., Quantitative Reflection Interference Contrast Microscopy (RICM) in Soft Matter and Cell Adhesion. *ChemPhysChem* **2009,** *10* (16), 2752-2768.

3. Contreras-Naranjo, J. C.; Silas, J. A.; Ugaz, V. M., Reflection interference contrast microscopy of arbitrary convex surfaces. *Appl. Opt.* **2010,** *49* (19), 3701-3712.

4. Ingham, D.B.; Yan, B. Re-entrainment of Particles on the Outer Wall of a Cyclindrical Blunt Sampler. *J. Aerosol. Sci.* **1994,** 25, 327-340**.**

5. Chang, J. Final Report, 2011 REU Summer Research Program, Texas A&M University, 2011.

6. Merkus, H. G., *Particle Size Measurements: Fundamentals, Practice, Quality*. Springer: 2009.

7. Pyrz, W. D.; Buttrey, D. J., Particle Size Determination Using TEM: A Discussion of Image Acquisition and Analysis for the Novice Microscopist. *Langmuir* **2008,** *24* (20), 11350-11360.

8. Stanley D. Duke, E. B. L., Improved Array Method for Size Calibration of Monodisperse Spherical Particles by Optical Microscope. *Thermo Scientific* **2000**.

9. Seitavuopio, P., *The Roughness and Imaging Characterisation of Different Pharmaceutical Surfaces*. University of Helsinki: 2006.

10. Chen, X.; Grattan, K. T. V.; Dooley, R. L., Optically interferometric roughness measurements for spherical surfaces by processing two microscopic interferograms. *Measurement* **2002,** *32* (2), 109-115.

11. Xiaohui Xu, Y. C., The Method of Spherical Surface Roughness Measurement. *Modern Applied Science* **2009,** *3* (12).

12. Bharat, B., Surface Roughness Analysis and Measurement Techniques. In *Modern Tribology Handbook, Two Volume Set*, CRC Press: 2000.

13. Weisstein, E. W. Beta Distribution. From *Mathworld*-A Wolfram Web Resource. http://mathworld.wolfram.com/BetaDistribution.html.

14. Atkinson, J. T.; Lalor, M. J., The effect of surface roughness on fringe visibility in optical interferometry. *Optics and Lasers in Engineering* **1980,** *1* (2), 131-146.